Accepted Manuscript

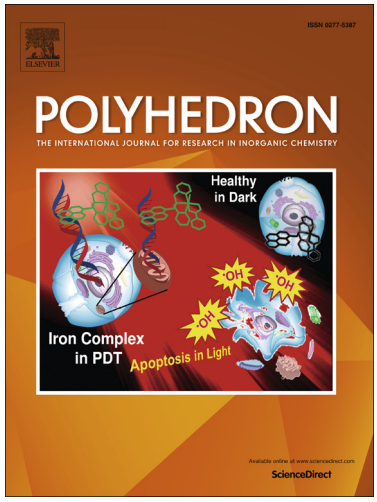

Synthesis, structural and corrosion inhibition studies on Mn(II), Cu(II) and Zn(II) complexes with a Schiff base derived from 2-hydroxypropiophenone

Monika Mishra, Karishma Tiwari, Ashish Kumar Singh, Vinod P. Singh

PII: S0277-5387(14)00213-7
DOI: http://dx.doi.org/10.1016/j.poly.2014.04.003
Reference: POLY 10646

To appear in: *Polyhedron*

Received Date: 21 January 2014
Accepted Date: 2 April 2014

Please cite this article as: M. Mishra, K. Tiwari, A.K. Singh, V.P. Singh, Synthesis, structural and corrosion inhibition studies on Mn(II), Cu(II) and Zn(II) complexes with a Schiff base derived from 2-hydroxypropiophenone, *Polyhedron* (2014), doi: http://dx.doi.org/10.1016/j.poly.2014.04.003

Synthesis, structural and corrosion inhibition studies on Mn(II), Cu(II) and Zn(II) complexes with a Schiff base derived from 2-hydroxypropiophenone

Monika Mishra[a], Karishma Tiwari[a], Ashish Kumar Singh[b] and Vinod P. Singh[a*]

[a]*Department of Chemistry, Banaras Hindu University, Varanasi-221005 (India)*

[b]*Department of Chemistry, North West University (Mafikeng Campus), Mmabatho 2735, South Africa.*

A B S T R A C T

A Schiff base, 2-hydroxy-benzoic acid [1-(2-hydroxy-phenyl)-propylidene]-hydrazide (H_2hbpp) and its Mn(II), Cu(II) and Zn(II) complexes have been synthesized. These compounds have been characterized by different physico-chemical and spectroscopic techniques (UV-Vis, IR, NMR and ESI-Mass). The molecular structure of H_2hbpp and its Mn(II) and Zn(II) complexes are determined by single crystal X-ray diffraction technique. In Mn(II) and Cu(II) complexes, the ligand coordinates through azomethine-N, carbonyl-O and phenolate-O (2-hydroxypropiophenone) forming a mono-nuclear 6-coordinate distorted octahedral geometry around metal. However, Zn(II) complex forms a phenoxo-bridged centrosymmetric dimer with 5-coordinate distorted square pyramid geometry around each metal ion. In this complex, the ligand bonds through azomethine-N, carbonylate-O and two phenolate-O, and a DMSO molecule occupies one of the vacant site of each metal. The structure of Cu(II) complex has been satisfactorily modeled by density functional theory (DFT) and time dependent-DFT (TD-DFT) calculations. The corrosion inhibition study of the synthesized compounds for mild steel in 1 M HCl medium has also been performed and the activity is found in the order: H_2hbpp < Cu(II) complex < Mn(II) complex < Zn(II) complex.

[*]Corresponding author. Tel.: +919450145060

E-mail address: singvp@yahoo.co.in (V.P. Singh)

Keywords: Transition metal complexes; Schiff base; 2-Hydroxypropiophenone; Single crystal X-ray diffraction study; Corrosion inhibition properties.

1. Introduction

The transition metal complexes with polydentate Schiff base ligands have developed an area of immense interest in coordination chemistry due to their variable bonding and structural possibilities, and their applications in several fields [1,2]. Aroylhydrazone Schiff bases are known to be a class of versatile ligands, capable of generating a variety of molecular architectures and coordination polyhedra [3-5]. The metal complexes of such Schiff bases have been extensively used as biological probes [6], DNA cleaving agents [7], catalysts [8,9], sensing materials [10,11] and corrosion inhibitors [12]. The biological activity of these complexes has been found to be highly dependent on the coordination behavior of metal ions and the binding sites on the ligands [13]. A survey of the literature reveals that many metallo-hydrolases contain binuclear Zn(II) complexes at their active sites [14]. Some Zn(II) based synthetic models having potential to mimic nucleases are also binuclear [15]. Recently, an oxo-bridged binuclear Mn(II) complex of oxaloyl dihydrazone has been reported to act as an excellent catalyst for transamidation of carboxamides with amines [16].

Schiff bases have been investigated as corrosion inhibitors for steel, copper and zinc [17-19]. Some research works have shown that the corrosion inhibition efficiency of Schiff bases is much greater than that of corresponding amines and aldehydes [20]. Due to presence of >C=N- groups, Schiff bases are adsorbed on the surface of mild steel and spontaneously form a monolayer on the surface, therefore, act as effective corrosion inhibitor [21,22]. The ability of Schiff base ligands to form stable complexes closely packed in the coordination sphere of metal ion, introduces another class of compounds for corrosion inhibition. The chelate environment with polyfunctional ligands, might plays a significant role in redox behavior and electro-catalytic reduction reactions. A few recent reports indicate that the metal

complexes show greater inhibition efficiency than the free ligands [23]. In view of the above, and only a very few reports available on the corrosion inhibition properties of transition metal complexes of aroylhydrazone Schiff bases, we have synthesized and characterized the Mn(II), Cu(II) and Zn(II) complexes with 2-hydroxy-benzoic acid[1-(2-hydroxy-phenyl)-propylidene]-hydrazide and studied their anti-corrosion properties on mild steel in acid solution. The experimental electronic and infrared spectral data of the copper(II) complex have also been compared with the theoretical data by DFT and TDDFT calculations.

2. Experimental

2.1 Materials and methods

All analytical grade chemicals were obtained from the commercial sources and used without further purification. 2-hydroxypropiophenone was purchased from Sigma–Aldrich, USA. Methyl salicylate, hydrazine hydrate (SD Fine Chemicals, India) and solvents (Merck Chemicals, India) were used as such. The precursor salicylic acid hydrazide, $(OH)C_6H_4CONHNH_2$ was prepared by the literature procedure [24].

2.2 Preparation of 2-hydroxy-benzoic acid [1-(2-hydroxy-phenyl)-propylidene]-hydrazide (H_2hbpp)

The ligand H_2hbpp was synthesized by reacting 25 ml methanolic solution of salicylic acid hydrazide (10 mmol, 1.52 g) with 25 ml methanolic solution of 2-hydroxypropiophenone (10 mmol, 1.50 ml) in a round bottom flask. The reaction solution was refluxed for 3 hours. A pale yellow product was obtained on cooling the above solution at room temperature. The product was filtered on a Büchner funnel and washed several times with methanol. The pure compound was recrystallised from hot methanol and dried in a desiccator over anhydrous calcium chloride at room temperature. Yield (77%). M.p. 240 ^oC. *Anal*. Calc. for $C_{16}H_{16}N_2O_3$ (284.31): C, 67.59; H, 5.67; N, 9.85. Found: C, 67.43; H, 5.69; N, 9.80%. IR (ν cm^{-1}, KBr): ν(O–H) 3448b, ν(N–H) 3294m, ν(C=O) 1638s, ν(C=N) 1610s, ν(N–N) 950w. ^{1}H NMR data:

1.23 (3H, J = 7.2 Hz, CH_3); 2.90 (2H, CH_2), 6.903-8.005 (Ar-H), 11.68 (s, 1H, NH), 13.19 (s, 1H, OH). ^{13}C NMR (DMSO-d_6): 11.05 (CH_3); 21.22(CH_2); 113.47-132.84 (Aromatic carbons); 163.01 (C=N); 166.76 (C-OH); 185.27 (C=O). The single crystal structure of the ligand was further confirmed by XRD.

2.3. Synthesis of the metal complexes

Mn(II), Cu(II) and Zn(II) complexes of H_2hbpp were synthesized by reacting 50 ml methanolic solution of each metal(II) acetates (5 mmol), separately with a solution of H_2hbpp (10 mmol, 2.84 g) in 25 ml hot methanol in 1:2 (M:L) molar ratio in a round bottom flask. The Mn(II) and Zn(II) complexes were formed as insoluble precipitates after refluxing the reaction mixture for 4 h, whereas, Cu(II) complex was precipitated immediately on stirring at room temperature. The metal complexes were filtered in a glass crucible, washed several times with methanol and finally with diethyl ether, and dried in a desiccator at room temperature. The single crystals of Mn(II) and Zn(II) complexes were obtained by slow diffusion of diethyl ether over a DMSO solution of the complexes.

2.3.1. [Mn(Hhbpp)$_2$]

Brown, yield (75%). M.p. 310^{d} ^{o}C. μ_{eff} = 5.96 B.M. *Anal*. Calc. for $C_{32}H_{30}MnN_4O_6$ (621.5): C, 61.84; H, 4.87; N, 9.01; Mn, 8.84. Found: C, 61.77; H, 4.84; N, 9.04; Mn, 8.80%. IR (ν cm^{-1}, KBr): ν(O–H), 3432b; ν(N–H), 3280m; ν(C=O), 1618s; ν(C=N), 1589s; ν(C-O^{-}), 1360s; ν(N–N), 985w; ν(M–O), 543w; ν(M–N), 419w. The single crystal structure of the complex was further confirmed by XRD.

2.3.2. [Cu(Hhbpp)$_2$]

Green, yield (74%). M.p. 260^{d} ^{o}C. μ_{eff} = 1.73 B.M. *Anal*. Calc. for $C_{32}H_{30}CuN_4O_6$ (630.15): C, 60.99; H, 4.80; N, 8.89; Cu, 10.08. Found: C, 60.88; H, 4.83; N, 8.85; Cu, 10.02%. IR (ν cm^{-1}, KBr): ν(O–H), 3438b; ν(N–H) 3294m; ν(C=O), 1630s; ν(C=N), 1599s;

ν(C-O$^-$), 1367s; ν(N−N), 990w; ν(M−O), 532w; ν(M−N) 425w. ESI-MS (calcd): *m/z* 630.152 [(M)$^+$, 12%]$^-$; 285.122 [(L+1)$^+$, 10%].

2.3.3. [Zn(hbpp)(DMSO)]$_2$

Yellow, yield (77%). M.p. 250^d ^{o}C. *Anal*. Calc. For $C_{36}H_{40}Zn_2N_4O_8S_2$ (851.6): C, 50.77; H, 4.73; N, 6.58; Zn, 15.35. Found: C, 50.68; H, 4.71; N, 6.54; Zn, 15.40%. IR (ν cm^{-1}, KBr): ν(O−H), 3428b; ν(C=N), 1585s; ν(C-O$^-$), 1355s; ν(N−N), 982w; ν(S=O), 915m; ν(M−O), 538w; ν(M−N), 425w. ^{1}H NMR data: 1.23 (3H, CH_3), 2.49 (2H, CH_2, J = 8.1 Hz), 6.49-8.73 (Ar-H), 14.07(s, 1H, OH), ^{13}C NMR (DMSO-d_6): 11.14 (CH_3); 22.76 (CH_2); 116.40-132.87 (Aromatic carbons); 163.28 (C=N); 167.50 (C-OH). The single crystal structure of the complex was further confirmed by XRD.

2.4 Physico-chemical measurements

The metal contents were analyzed gravimetrically by the literature procedure [25]. Carbon, hydrogen and nitrogen contents were determined on an Exeter Analytical Inc. CHN Analyzer (Model CE-440). ^{1}H NMR spectra of the ligand and its Zn(II) complex were recorded in DMSO-d_6 on a JEOL AL-300 FT-NMR multinuclear spectrometer. Chemical shifts were reported in parts per million (ppm) using tetramethylsilane (TMS) as an internal standard. Infrared spectra were recorded in KBr on a Varian 3100 FT-IR spectrophotometer in the 4000-400 cm^{-1} region. Electronic spectra of the complexes were recorded on a Shimadzu spectrophotometer, model, Pharmaspec UV-1700 in DMSO as solvent. Magnetic susceptibility measurements were performed at room temperature on a Faraday balance using Hg[Co(SCN)$_4$] as the calibrant. ESI-Mass spectrometric analysis was carried out on a Waters-Q-Tof Premier-HAB213 mass spectrometer.

2.5. Crystal structure determination

Single crystal X-ray diffraction data for the ligand H_2hbpp and its Mn(II) and Zn(II) complexes were obtained at 293(2) K, on a Oxford Diffraction Gemini Diffractometer equipped with CrysAlis Pro., using a graphite mono-chromated Mo $K\alpha$ (λ = 0.71073 Å) radiation source. The structures were solved by direct method (SHELXL-97) and refined against all data by full matrix least-square on F^2 using anisotropic displacement parameters for all non-hydrogen atoms. All hydrogen atoms were included in the refinement at geometrically ideal position and refined with a riding model [26,27]. The Mercury and ORTEP-3 software packages for windows program were used for generating structures [28,29].

2.6. Computational studies.

All calculations were performed for the Cu(II) complex using *Gaussian-09* suit of programs. The complex was treated as an open-shell system using spin unrestricted DFT wave functions (UB3LYP) [30], i.e. the Becke three-parameter exchange functional in combination with the LYP correlation functional of Lee, Yang and Parr with 6-31G (d,p) basis set for C, H, N and O atoms [31] and effective core potentials basis set LanL2DZ (Los Alamos National Laboratory 2 double zeta) [32] for the Cu atom. The optimized structure was confirmed to be minima on potential energy surface (PES) by performing harmonic vibration frequency analyses (no imaginary frequency found). No symmetry constraints were applied and only the default convergence criteria were used during the geometry optimizations. Based on the optimized geometries, TDDFT calculations were performed at the same UB3LYP level to calculate the vertical electronic transition energies.

2.7. Corrosion inhibition measurements

Prior to all measurements, the mild steel specimen of composition (wt %) C = 0.17, Mn = 0.46, Si = 0.26, S = 0.017, P = 0.019 and balance Fe, was abraded successively with emery papers. The aggressive solution of 1 M HCl was prepared by dilution of analytical

148 grade HCl (37%) with double distilled water and all experiments were carried out in unstirred
149 solutions. The rectangular specimens with dimension 2.5 × 2.0 × 0.025 cm^3 was used in
150 weight loss experiments and of size 1.0 ×1.0 cm^2 (exposed) with a 7.5 cm long stem (isolated
151 with commercially available lacquer) was used for electrochemical measurements [33]. Stock
152 solutions of studied inhibitors were made in 10:1 (water: DMSO) ratio by volume to ensure
153 solubility. These stock solutions were used for all experimental purposes.

154 The electrochemical measurements were done by method described earlier [20]. A
155 three-electrode cell, consisting of carbon steel working electrode (WE), a platinum counter
156 electrode (CE), and saturated calomel electrode (SCE) as a reference electrode, was used for
157 electrochemical measurements. All experiments were performed in atmospheric condition
158 without stirring. Prior to the electrochemical measurement, a stabilization period of 30 min
159 was allowed, which was proved to be sufficient to attain a stable value of E_{corr}. The EIS
160 measurements were carried out in a frequency range from 100 kHz to 0.00001 kHz under
161 potentiostatic conditions, with amplitude of 10 mV peak-to-peak, using the AC signal at E_{corr}.
162 The potentiodynamic polarization curves were recorded in the potential range of −250 to
163 +250 mV (SCE) with a scan rate of 1 mV s^{-1}. All potentials were measured against SCE.

164 The inhibition efficiencies have been calculated from EIS and current density (i_{corr})
165 from the following equations.

166
$$E_{EIS}\% = \frac{R_p^i - R_p^0}{R_p^i} \times 100 \quad (1)$$

$$E_{PDP}\% = \frac{i_{corr}^0 - i_{corr}^i}{i_{corr}^0} \times 100 \quad (2)$$

167 where R_p^i & R_p^0 are the polarization resistances and i_{corr}^0 & i_{corr}^i are the current density in
168 presence and absence of inhibitors, respectively.

3. Results and discussion

The analytical data of metal complexes reveal that although the reactions between metal(II) acetates and the ligand are performed in 1:2 (M:L) molar ratio, only Mn(II) and Cu(II) forms 1:2 (M:L) complexes. The Zn(II) forms a 1:1 (M:L) dimer under similar conditions. In all the metal(II) complexes, hydroxyl-proton of 2-hydroxy propiophenone deprotonates during complexation and the ligand bonds through phenolate-O to metal. In Zn(II) complex, phenolate-O bridges between two metal atoms resulting into a dimeric structure for the complex. In addition, the carbonyl-O of the ligand enolizes during complexation and deprotonates to bond through carbonylate-O. The solvent DMSO also occupies one of the vacant site of each Zn(II) giving a 5-coordinate distorted square pyramid geometry around metal ion. The reactions are given in Scheme 1.

The metal complexes are intensely colored solids and thermally stable upto 250 ^{o}C. They are insoluble in water and common organic solvents viz. ethanol, methanol, chloroform, benzene, cyclohexane, acetone and diethyl ether but are soluble in DMF and DMSO. The Mn(II) and Zn(II) complexes have been successfully crystallized to get their single crystals in DMSO solvent. However, in spite of all the efforts, Cu(II) complex could not be crystallized.

3.2. *Electronic spectra and magnetic moments*

The intense absorption band observed at 331 nm in the spectrum of ligand is predominantly due to n→π* transitions associated with azomethine chromophore. The other intense band located in the high-energy region at 291 nm is due to π→π* transition of aromatic rings of the free ligand [34]. These transitions are also observed in the spectra of metal complexes with a slight shift in wavelength, indicating coordination of the ligand to metal centre. In the electronic spectra of metal complexes, one new band appears in the region 406–393 nm, may be assigned to a mixed ligand-to-ligand (LLCT) and ligand-to-metal (LMCT) charge transfer transitions [35,36].

The Cu(II) complex exhibits a broad d-d transition band centered at 653 nm, attributable to the $^2T_{2g} \leftarrow {}^2E_g$ transition suggesting a distorted octahedral geometry [37]. The complex shows μ_{eff} value 1.73 B.M., corresponding to one unpaired electron [38]. The Mn(II) complex shows a band of weak intensity at 640 nm, which may be assigned to $^6A_{1g} \rightarrow {}^4T_{1g}$ transition in an octahedral environment [23]. The magnetic moment value, 5.96 B.M. observed for Mn(II) complex, suggests the presence of five unpaired electrons [39].

3.3. ^1H and ^{13}C NMR

The resonance signals due to two Ar-OH and –NH protons appear in the ligand H_2hbpp at 13.19 and 11.68 ppm, respectively (Fig. S1). One of the Ar-OH signal shows a downfield shift in the Zn(II) complex and occurs at 14.07 ppm due to its involvement in intra-molecular hydrogen bonding, whereas, the other disappears due to deprotonation. The –NH proton signal of the ligand also disappears in its Zn(II) complex as a result of enolization of >C=O group during complexation (Fig. S2).

^{13}C NMR spectrum of ligand shows the signals at 11.05, 21.22, 163.01, 166.76 and 185.27 ppm, attributed to $–CH_3$, $>CH_2$, >C=N, C–OH and >C=O carbons, respectively (Fig. S3). The Zn(II) complex shows a downfield shift for >C=N carbon signal which appears at 163.28 ppm, suggesting the bonding of >C=N group with metal ion. The absence of a >C=O signal in Zn(II) complex indicates enolization of >C=O group (Fig. S4). The signals due to C-OH and C-O$^-$ appear at the same position at 167.50 ppm in the complex.

3.4. Mass spectra

The ESI-MS spectra of the Cu(II) complex exhibits a number of peaks due to formation of various fragments of the complex. The molecular ion peak observed at m/z = 630.152 with 12% intensity matches well with the molecular weight calculated for the Cu(II) complex. The peak observed at *m*/*z* = 285.12 with 10% intensity, corresponds to the formula weight of ligand (Fig. S5).

3.1. IR spectra

The ν(N-H) observed at 3294 cm^{-1} in the IR spectrum of free ligand, occurs nearly at the same or at a slightly shifted position in its Mn(II) and Cu(II) complexes, indicating the non-involvement of >NH group in bonding [29]. The ν(C=O) band observed at 1638 cm^{-1} in the ligand, is shifted to lower wave number by 10-18 cm^{-1} in its Mn(II) and Cu(II) complexes, indicating coordination of the >C=O group to the metal ion [40]. However, the disappearance of ν(C=O) and ν(N-H) bands in Zn(II) complex, suggests the involvement of >C=O group in enolization, which deprotonates during complexation. The appearance of a new $\nu(C\text{-}O)^-$ band in all the metal complexes in the range 1360-1355 cm^{-1}, suggests bonding of the ligand to metal through a phenolate-O [41]. The ν(C=N) band observed at 1610 cm^{-1} in the spectra of ligand, shifts to lower frequency (11-25 cm^{-1}) in all the metal complexes, suggesting coordination of azomethine-N. Moreover, a new >C=N- band appears at 1603 cm^{-1} in the Zn(II) complex due to enolization of >C=O group. A weak band due to ν(N-N) observed at 950 cm^{-1} in the ligand, shifts to higher frequency by 32-40 cm^{-1} in its metal complexes, indicating the coordination of one of the nitrogen atom of the N-N group with metal [23]. The ligand and its metal complexes also show a broad band in the 3448-3428 cm^{-1} region due to phenolic–OH group [42]. The non-ligand bands in the 543-532 cm^{-1} and 425-419 cm^{-1} ranges have been tentatively assigned to ν(M-O) and ν(M-N), respectively. The band observed at 915 cm^{-1} in the Zn(II) complex, is assigned to ν(S=O) of coordinated DMSO molecule [43].

3.5.1. Crystal structure of H_2hbpp

Fig. 1 shows the ORTEP diagram of the ligand with atomic numbering scheme. The crystallographic data, structural refinement details of the ligand and the complexes are given in Table 1. Selected bond lengths, bond angles and hydrogen bonding parameters of the ligand and the complexes are given in Tables 2 and 3. The bond lengths of O(1)–C(7) and C(7)–N(1) are 1.245(5) and 1.351(5) Å, respectively, which correspond to typical double

bonds. The N(1)–N(2) bond distance is 1.356(5) Å, which is slightly shorter than the single bond distance (~1.411(7) Å) reported previously, indicating some double bond character [44]. The torsion angles O(1)–C(7)–N(1)–N(2), 3.2(6)°, C(8)–C(9)–C(10)–O(3), -1.4(8)° and C(2)–C(1)–C(7)–O(1), 176.4(4)° indicate that the O(1) and N(2), and C(8) and O(3) are *syn-periplanar* to each other, while C(2) and O(1) are *anti-periplanar* to each other. Crystal packing of H_2hbpp is stabilized by N(1)–H(1)···O(2), O(3)–H(3)···N(2) intra-molecular and O(2)–H(2A)···O(1), C(3)–H(3A)···O(1) inter-molecular interactions (Fig. S6).

Table 1

Selected crystallographic data of H_2hbpp, $[Mn(Hhbpp)_2]$ and $[Zn(hbpp)(DMSO)]_2$

	H_2hbpp	$[Mn(Hhbpp)_2]$	$[Zn(hbpp)(DMSO)]_2$
Empirical formula	$C_{16}H_{16}N_2O_3$	$C_{32}H_{30}MnN_4O_6$	$C_{36}H_{40}N_4O_8S_2Zn_2$
Formula weight	284.31	621.54	851.58
T (K), λ (Å)	293(2), 0.71073	293(2), 0.71073	293(2), 0.71073
Crystal system	Monoclinic	monoclinic	Monoclinic
Space group	P 2_1/c	C2/c	P 2_1/c
Unit cell dimensions	a = 12.9138(18)	a = 22.4052(13)	a = 12.7873(3)
	b = 13.1039(18)	b = 9.6538(6)	b = 14.7998(4)
	c = 8.2523(17)	c = 13.6650(8)	c = 10.2523(3)
	β = 93.164(17)	β = 99.850(5)	β = 93.175(2)
Volume ($Å^3$), Z	1394.3(4), 4	2912.1(3), 4	1937.26(9), 2
Density (mg/m^3)	1.354	1.418	1.460
Absorption coefficient (mm^{-1})	0.095	0.505	1.400
F(000)	600	1292	880
Crystal size (mm^3)	0.25 x 0.23 x 0.20	0.25 x 0.24 x 0.21	0.23 x 0.21 x 0.20

Theta range for data collection	2.91 - 29.13	3.03 - 29.03	2.96 - 29.18
Index ranges	-15 ≤ h ≤ 17,	-20 ≤ h ≤ 30	-7 ≤ h ≤ 17
	-17 ≤ k ≤ 15	-13 ≤ k ≤ 7	-18 ≤ k ≤ 16
	-10 ≤ l ≤11	-17 ≤ l ≤ 15	-13 ≤ l ≤ 13
Reflections collected /unique	4604 / 3752	6254/3882	8929 / 5230
	[R_{int} = 0.0459]	[R_{int} = 0.0393]	[R_{int} = 0.0247]
Data/restraints/parameters	3752 / 0 / 194	3882 / 2 / 197	5230 / 0 / 239
Goodness-of-fit on F^2	0.950	1.047	1.018
R_1, wR_2 [a,b][(I>2σ(I))]	0.0834, 0.1653	0.0605, 0.0914	0.0395, 0.0832
R_1, wR_2 [a,b] (all data)	0.2193, 0.2428	0.1128, 0.1085	0.0629, 0.0957
Residual electron density(e Å^{-3})	0.292, -0.209	0.399, -0.450	0.333, -0.425

253 [a] $R_1 = \Sigma||F_o| - |Fc||\Sigma|F_o|$.

254 [b] $R_2 = [\Sigma w(|F^2_o| - |F^2_c|)^2/\Sigma w|F^2_o|^2]^{1/2}$

255 **Table 2**

256 Selected bond lengths and angles of H_2hbpp, [Mn(Hhbpp)$_2$], [Zn(hbpp)(DMSO)]$_2$

H_2hbpp		[Mn(Hhbpp)$_2$]		[Zn(hbpp)(DMSO)]$_2$	
Bond lengths (Å)					
		Mn-O(1)	1.909(2)	Zn-O(3)	1.9936(17)
		Mn-O(3)	1.829(2)	Zn-O(4)	2.0054(19)
		Mn-N(2)	1.962(2)	Zn-O(1)	2.0342(17)
O(1)-C(7)	1.245(5)	O(2)-C(2)	1.347(4)	Zn-O(3a)	2.0424(17)
O(3)-C(10)	1.348(6)	O(1)-C(7)	1.297(3)	Zn-N(2)	2.063(2)
O(2)-C(2)	1.362(6)	O(3)-C(10)	1.336(3)	O(3)-C(10)	1.346(3)
N(1)-C(7)	1.351(5)	N(1)-C(7)	1.306(3)	O(1)-C(7)	1.274(3)

N(1)-N(2)	1.356(5)	N(1)-N(2)	1.377(3)	N(1)-N(2)	1.394(3)
N(2)-C(8)	1.277(6)	N(2)-C(8)	1.307(3)	C(7)-N(1)	1.320(3)
				N(2)-C(8)	1.293(3)
				Zn-Zn(a)	3.1209(6)
Bond angles (°)					
C(8)-N(2)-N(1)	120.8(4)	O(1)-Mn-O(3)	171.03(7)	O(1)-Zn-O(3)	104.17(7)
C(7)-N(1)-N(2)	120.9(4)	O(3)-Mn-N(2)	90.68(9)	O(1)-Zn-N(2)	78.81(7)
O(1)-C(7)-N(1)	119.4(5)	O(1)-Mn-N(2)	80.65(9)	O(1)-Zn-O(4)	100.24(8)
O(1)-C(7)-C(1)	122.2(5)	O(1)-Mn-O(3a)	89.65(9)	O(3)-Zn-O(4)	106.22(9)
N(2)-C(8)-C(9)	117.9(5)	N(2a) -Mn-N(2)	169.65(16)	O(4)-Zn-N(2)	112.71(9)
		N(2)-Mn-O(1a)	92.19(9)	O(3)-Zn-N(2)	139.81(8)
		O(3)-Mn-O(3a)	89.07(15)	O(1)-Zn-O(3a)	158.51(8)
		O(1)-Mn-O(1a)	92.96(13)	O(3)-Zn-O(3a)	78.71(7)
				N(2)-Zn-O(3a)	85.46(7)
				Zn-O(3)-Zn(a)	101.29(7)
				O(4)-Zn-O(3a)	99.29(8)

'a' refers to the elements generated by symmetry operation = -x+1, y, -z+3/2 for [Mn(Hhbpp)$_2$] and -x+2, -y, -z for [Zn(hbpp)(DMSO)]$_2$**.**

Table 3

Hydrogen bond parameters [Å and ˚] of H_2hbpp, [Mn(Hhbpp)$_2$] and [Zn(hbpp)(DMSO)]$_2$

H_2hbpp				
D–H···A	D–H	H···A	D···A	< (DHA)
N(1)–H(1)–O(2)	0.86	1.96	2.642(6)	135
O(3)–H(3)–N(2)	0.82	1.83	2.548(6)	146

O(2)–H(2A)···O(1)$^{\#1}$	0.82	1.90	2.705(6)	168
C(3)–H(3A)···O(1)$^{\#1}$	0.93	2.44	3.154(7)	134
C(6)–H(6)···O(1)	0.93	2.46	2.793(7)	101
$^{\#1}$ = 1-x,1/2+y,1/2-z				
[Mn(Hhbpp)$_2$]				
N(1)–H(1)···O(2)	0.86	1.94	2.570(4)	129
C(6)–H(6)···O(1)	0.93	2.45	2.774(4)	100
C(6)–H(6)···O(2)$^{\#1}$	0.93	2.59	3.319(3)	136
$^{\#1}$ = x,-y,1/2+z				
[Zn(hbpp)(DMSO)]$_2$				
O(2)–H(2)···N(1)	0.82	1.79	2.523(3)	148
C(6)–H(6)···O(1)	0.93	2.48	2.794(3)	100
C(11)–H(11)···O(1)	0.93	2.39	3.166(3)	141
C(14)–H(14)···O(4)$^{\#1}$	0.93	2.56	3.335(3)	141
$^{\#1}$ = x,1/2-y,-1/2+z				

3.5.2. Crystal structure of [Mn(Hhbpp)$_2$]

The ORTEP diagram of the Mn(II) complex with atomic numbering scheme is given in Fig. 2. The Mn(II) metal ion is coordinated to two mono-anionic ligands through a carbonyl-O, azomethine-N and a phenolate-O of each ligands. The molecular structure shows a distorted octahedral geometry around metal ion and structure has crystallographic twofold symmetry. In complex, the carbonyl-O and phenolate-O of the two ligands are cis to each other and two azomethine-N are trans to each other. The Mn-O(1) (carbonyl-O), Mn-O(3) (phenolate-O) and Mn-N(2) (azomethine-N) bond lengths are 1.909(2), 1.829(2) and 1.962(2) Å, respectively [23,45,46]. These bond lengths fall in the normal range of many octahedral

Mn(II) complexes with N,O–donor ligands. The shorter Mn–O(3) bond length as compared to Mn–O(1) indicates that the phenolate-O bond is more stronger than the carbonyl oxygen [47]. The observed bond angles N(2)-Mn-O(1), 80.65(9)°; O(3)-Mn-N(2), 90.68(9)° and O(1)-Mn-O(3), 171.03(7)° indicate that the octahedral geometry is slightly distorted due to chelation effect [41,48]. The torsion angles O(1)–C(7)–N(1)–N(2), 5.4(4)°, N(1)–N(2)–C(8)–C(15), 1.2(4)° and C(14)–C(9)–C(8)–N(2), 169.3(3)°, indicate that the O(1) and N(2), and N(1) and C(15) are *syn-periplanar* to each other, while C(14) and N(2) are *anti-periplanar* to each other. The molecule forms a butterfly like architecture along '*c*' axis through N(1)–H(1)···O(2) and C(6)–H(6)···O(1) intra-molecular and C(6)–H(6)···O(2) inter-molecular hydrogen-bonding interactions (Table 3, Fig. S7).

3.5.3. Structure of [Zn(hbpp)(DMSO)]$_2$

Fig. 3 shows the ORTEP diagram of Zn(II) complex with atomic numbering scheme. The crystal structure shows that Zn(II) complex is a phenoxo-bridged centrosymmetric dimer having 5-coordinate distorted square-pyramid geometry in which metal bonds through an azomethine-N, carbonylate-O and two bridged phenolate-O of the ligands at the base, and a sulfoxide-O of DMSO molecule occupies the apical position. The C(8)–N(2) distance (1.293(3) Å) in the complex is longer than in the ligand (1.277(6) Å) due to coordination of azomethine-N to the metal ion. The N(1)–C(7) distance (1.320(3) Å) in the complex is significantly shorter than in the free ligand (1.351(5) Å) as a result of deprotonation of imine group and formation of >C=N. The O(1)–C(7) bond length (1.274(3) Å) is also longer in the complex than the free ligand (1.245(5) Å) due to enolization of >C=O group during complexation [16]. The bond distances for Zn–N(2), Zn–O(1), Zn–O(3) and Zn–O(4) are 2.063(2), 2.0342(17), 1.9936(17) and 2.005(19) Å respectively, which are comparable to the bond lengths reported for similar Zn(II) complexes in literature [47,49]. O(1)-Zn-N(2), 78.81(7)°; O(1)-Zn-O(3), 104.17(7)°; O(1)-Zn-O(4), 100.24(8)°; O(3)-Zn-O(4), 106.22(9)°;

O(3)-Zn-N(2), 139.81(8)°; O(4)-Zn-N(2), 112.71(9)° bond angles are also comparable to other reported distorted square pyramid Zn(II) complexes with N,O-donor ligands [50]. The torsion angles O(1)–C(7)–N(1)–N(2), 1.1(4)°, C(15)–C(8)–N(2)–N(1), 3.5(4)° and C(14)–C(9)–C(8)–N(2), 157.5(2)° indicate that O(1) and N(2), and C(15) and N(1) are *syn-periplanar* to each other but C(14) and N(2) are *anti-periplanar* to each other. Crystal packing structure of the complex is stabilized by intra-molecular O(2)–H(2)···N(1), C(6)–H(6)···O(1) and C(11)–H(11)···O(1) and inter-molecular C(14)–H(14)···O(4) hydrogen-bonding interactions (Table 3, Fig. S8).

3.6. DFT optimized structure of [Cu(Hhbpp)$_2$]

The density functional theory calculations were carried out in gas phase to optimize the structure of Cu(II) complex, using coordinates of the crystal structure of Mn(II) complex from the CIF file. The DFT optimized structure is shown in Fig. 4. The selected bond lengths and bond angles of the complex are given in Table S1. The bond distances Cu-N(2), Cu-N(4), Cu-O(1), Cu -O(4), Cu-O(3), and Cu-O(6) are 2.296, 2.295, 2.173, 2.171, 1.927 and 1.926 Å, are comparable to the bond lengths reported for similar Cu(II) complexes in literature (Table S1) [51, 52]. The observed bond angles around the metal centre agree reasonably well with other reported Cu(II) complexes of N,O donor ligands in distorted octahedral system [53]. The bond lengths O(1)–C(7), O(4)–C(23), C(8)–N(2) and C(24)–N(4) are 1.218, 1.218, 1.274 and 1.274 Å respectively, which correspond to typical double bond characteristic.

The experimental IR spectral data for the Cu(II) complex have been correlated with the DFT calculated data based on peak intensities and peak frequencies (cm^{-1}) (Table S2). Apart from some minor deviations in theoretical group frequencies from the experimental (6-16 cm^{-1}), the theoretical–experimental agreement is satisfactory. Little deviations are due to the negligence of anharmonicity in B3LYP method [54] and average error in frequencies calculated with B3LYP method is reported to be of the order of 40-50 cm^{-1} [55].

In order to get a deeper understanding of the electronic transitions, TDDFT calculations have been performed for the Cu(II) complex. The assignments of the calculated transitions to the experimental bands are based on the criteria of energy and oscillator strength of the calculated transitions. In the description of the electronic transitions, only the main components of the molecular orbitals are taken into consideration. The calculated absorption bands for the complex are shown by the vertical lines in Fig. S9, S10 and the band assignments are given in Table S3 with their oscillator strengths and energies. The results of time-dependent density functional theory (TDDFT) calculations on Cu(II) complex at the UB3LYP level reveal that the band calculated in the region 310-380 nm is due to mixed ligand→metal (LMCT) and intra-ligand (ILCT) charge transfer transitions. The other low energy absorption band at 657 nm is due to d-d transition with smaller oscillator strength. The orbital analysis of above d-d transiton suggests that it originates from d_z^2, $d_{x^2-y^2}$ to d_{xy}, d_{yx}, d_{xz} orbitals, as expected for a distorted octahedral copper(II) complex (Fig. S11).

3.8. Corrosion inhibition efficiency

3.8.1. Electrochemical impedance spectroscopy (EIS)

Electrochemical impedance spectroscopy is a rapid and convenient method for investigation of protective properties of corrosion inhibitors on metals. More reliable results can be obtained by this method, since it does not disturb the double layer at the metal/solution interface [56]. Consequently, EIS is specially a useful method to follow the evaluation of inhibitor–metal system over time [57]. The effect of inhibitor concentration on mild steel was studied by using EIS measurements in 1 M HCl in the absence and presence of studied compounds at 303 K. The impedance plots and proposed equivalent electrical circuit of mild steel in 1 M HCl in absence and presence of studied compounds are presented in Fig. 5. The main parameters (R_f, R_{ct}, Y_0 and n) deduced from the analysis of Nyquist diagrams for 1 M

HCl containing various concentrations of Oxandra asbeckii plant extract (OAPE) are given in Table 4.

Table 4

Impedance parameters for mild steel in absence and presence of studied inhibitors.

Inhibitor	Conc. of Inhibitor (ppm)	R_s (Ω cm^2)	Y_0 (10^{-6} Ω^{-1} S^n cm^{-2})	n	L (H)	R_{ct} (Ω cm^2)	R_L(Ω cm^2)	E_{EIS}%
-	-	1.01	180	0.821	11.9	35.8	10.2	-
H_2hbpp	50	0.91	141	0.835	10.8	281.8	25.1	85.0
[Mn(Hhbpp)$_2$]	50	0.85	84	0.855	8.4	367.4	28.6	88.4
[Cu(Hhbpp)$_2$]	50	0.96	101	0.851	9.9	332.6	18.2	86.9
[Zn(hbpp)(DMSO)]$_2$	50	0.92	71	0.871	8.1	505.2	47.2	91.7

Fig. 5 shows the Nyquist plots for mild steel in electrolyte solution in absence and presence of 50 mg L^{-1} of studied compounds at 303 ± 1 K. The Nyquist plots obtained for the corrosion of mild steel in HCl solution with inhibitor consist of two capacitive loops (two well-defined time-constants in the Bode-phase format) and an inductive loop. The high frequency (HF) capacitive loop, the smaller one, can be attributed to the film formation at the steel surface while the low frequency (LF) loop, the larger one, can be attributed to the charge transfer reaction. The presence of the LF inductive loop may be attributed to the relaxation process obtained by adsorption species like Cl^-_{ads} and H^+_{ads} on the electrode surface [58]. The phase angle at high frequency provides a general idea of anticorrosion performance of inhibitor. The more negative the phase angle shows more capacitive the electrochemical behaviour. To get a more accurate fit of these experimental data, the measured impedance data are analyzed by fitting in an equivalent circuit. Excellent fit with this model is obtained

for all experimental data. The equivalent circuit consists of the constant phase element (*CPE*) in parallel to the charge-transfer resistance (R_{ct}), which is in series to the parallel of inductive elements (L) and R_L. One constant phase element (CPE) is substituted for the capacitive element to give a more accurate fit, as the obtained capacitive loop is a depressed semicircle. The depression in Nyquist semicircles is a feature for solid electrodes and often referred to as frequency dispersion and attributed to the roughness and other inhomogenities of the solid electrode. For analysis of the impedance spectra exhibiting two capacitive loops and an inductive loop, the equivalent circuit shown in Fig. 6, was used to fit the experimental data.

3.8.2. Potentiodynamic polarization (PDP) measurements

Fig. 7 represents the potentiodynamic polarization curves of mild steel in 1 M HCl in the absence and presence of 50 ppm of the studied compounds. In the presence of inhibitors, the curves are shifted to lower current regions, showing the inhibition tendency of studied inhibitors. No definite trend is observed in the E_{corr} values in the presence of ceftobiprole. In the present study, a shift in E_{corr} values in the range of 2–22 mV suggests that they all act as mixed type of inhibitor. The values of various electrochemical parameters derived by Tafel polarization of the inhibitors are given in Table 5. Investigation of Table 5 reveals that the values of β_a change slightly in the presence of ceftobiprole. A more pronounced change in the values of β_c indicates that although both the anodic and cathodic reactions are effected, the effect on the cathodic reactions is more prominent. The inhibition efficiency depends on many factors including adsorption centers, mode of interaction, molecular size and geometry of the inhibitors. The adsorption behavior of the ligand H_2hbpp is argued to the presence of unshared electron pair on hetero atoms and π-electrons on aromatic rings. All the studied complexes as well as ligand increase the polarization resistance due to adsorption. The samples exposed to Zn(II) complex solution exhibits greatest inhibition among the other studied compounds. The complex formation between Zn(II) complex, iron oxide and

hydroxide is responsible for corrosion inhibition activity of this complex, resulting into precipitation of an insoluble compound on the surface and hence, further deterioration of metal is decreased. Similar behavior is observed with Mn(II) complex but due to its monomeric structure, inhibition effect caused by this complex is smaller compared to that of Zn(II) complex. The least inhibition efficiency of Cu(II) complex is due to its less negative electrode potential. The increased efficiency of metal complexes compared to the ligand may be attributed to their larger size. Thus, the inhibition efficiency of the studied compounds varies as H_2hbpp < Cu(II) complex < Mn(II) complex < Zn(II) complex.

Table 5

Potentiodynamic polarization parameters for mild steel in absence and presence of studied inhibitors.

Inhibitor	Conc. of Inhibitor/ppm	$-E_{corr}$ (mV *vs.* SCE)	i_{corr}(μA cm^{-2})	β_a (mV dec^{-1})	β_c(mV dec^{-1})	E_{PDP}%
-	-	469	731	73	127	-
H_2hbpp	50	470	121	71	137	83.4
[Mn(Hhbpp)$_2$]	50	478	87	77	139	88.1
[Cu(Hhbpp)$_2$]	50	465	104	72	138	85.8
[Zn(hbpp)(DMSO)]$_2$	50	481	64	79	140	91.2

.4. Conclusions

This paper describes the synthesis and characterization of a Schiff base derived from 2-hydroxypropiophenone and its Mn(II), Cu(II) and Zn(II) complexes. The molecular structures of the ligand H_2hbpp, Mn(II) and Zn(II) complexes have been determined by single crystal X-ray diffraction techniques. H_2hbpp acts as a monobasic tridentate ligand and coordinates through azomethine-N, carbonyl-O and phenolate-O with Mn(II) and Cu(II) ions

giving a distorted octahedral geometry. The Zn(II) complex forms a phenoxo-bridged centrosymmetric dimer with 5-coordinate distorted square pyramid geometry containing a DMSO molecule at apical position. The structure of Cu(II) complex has also been optimized by DFT and TDDFT calculations. Theoretical calculations suggest an agreement between theoretical and experimental analyses of electronic and infrared spectral data. The corrosion inhibition efficiency of the synthesized compounds was also studied for mild steel in 1 M HCl medium.

Appendix A. Supplementary data

The Figures S1-S11 and Table S1-S3 are available in supplementary materials. CCDC 939625, 878529 and 936392 contain the supplementary crystallographic data for H_2hbpp, [Mn(Hhbpp)$_2$] and [Zn(hbpp)(DMSO)]$_2$, respectively. These data can be obtained free of charge via http://www.ccdc.cam.ac.uk/conts/retrieving.html, or from the Cambridge Crystallographic Data Centre, 12 Union Road, Cambridge CB2 1EZ, UK; fax: (+44) 1223-336-033; or e-mail: deposit@ccdc.cam.ac.uk.

Acknowledgements

The authors thank the Head, S.A.I.F., Indian Institute of Technology, Kanpur, India for recording the ESI-mass spectra. One of the authors V.P.S. is grateful to UGC, New Delhi for financial assistance.

References

[1] E. Zangrando, M. Casanova, E. Alessio, Chem. Rev. 108 (2008) 4979–5013.

[2] S.J. Dalgarno, N.P. Power, J.L. Atwood, Coord. Chem. Rev. 252 (2008) 825–841.

[3] L.H. Uppadine, J.P. Gisselbrecht, J.M. Lehn, Chem. Commun. (2004) 718-719.

[4] L.H. Uppadine, J.M. Lehn, Angew. Chem. Int. Ed. 43 (2004) 240-243.

[5] C.R. Perez, J.G. Platas, H. Lotter, L. Lezama, X. Solans, S. Dominguez, P.M. Zarza, M.J. Rocio, M.S. Palacios, P. Gili, Inorg. Chim. Acta 255 (1997) 139–148.

[6] S. Banerjee, S. Mondal, S. Sen, S. Das, D.L. Hughes, C. Rizzoli, C. Desplanches, C. Mandal, S. Mitra, Dalton Trans. (2009) 6849–6860.

[7] R. Gaur, L. Mishra, Inorg. Chem. 51 (2012) 3059–3070.

[8] J.Y. Lee, O.K. Farha, J. Roberts, K.A. Scheidt, S.T. Nguyen, J.T. Hupp, Chem. Soc. Rev. 38 (2009) 1450–1459.

[9] D.P. Singh, D.S. Raghuvanshi, K.N. Singh, V.P. Singh, J. Mol. Catal. A: Chem. 379 (2013) 21–29.

[10] V.P. Singh, K. Tiwari, M. Mishra, N. Srivastava, S. Saha, Sens. Actuators, B 182 (2013) 546– 554.

[11] A. Sahana, A. Banerjee, S. Das, S. Lohar, D. Karak, B. Sarkar, S.K. Mukhopadhyay, A.K. Mukherjee, D. Das, Org. Bio. Chem. 9 (2011) 5523–5529.

[12] A.S. Fouda, M.M. Gouda, S.I. Abd El-Rahman, Bull. Korean Chem. Soc. 21 (2000) 1085-1089.

[13] D.E. Wilcox, Chem. Rev. 96 (1996) 2435-2458.

[14] G. Parkin, Chem. Rev. 104 (2004) 699-767.

[15] C. Liu, M. Wang, T. Zhang, H. Sun, Coord. Chem. Rev. 248 (2004) 147-168.

[16] D.P. Singh, B.K. Allam, K.N. Singh, V.P. Singh, RSC Adv. 4 (2014) 1155–1158.

[17] K.S. Jacob, G. Parameswaran, Corros. Sci. 52 (2010) 224–228.

[18] S. Li, S. Chen, S. Lei, H. Ma, R. Yu, D. Liu, Corros. Sci. 41 (1999) 1273–1287.

[19] A.S. Fouda, L.H. Madkour, A.A. El-Shafei, S.A. Abd El Maksoud, Bull. Korean Chem. Soc. 16 (1995) 454–458.

[20] A.K. Singh, Ind. Eng. Chem. Res. 51 (2012) 3215-3233.

[21] S. Li, S. Chen, H. Ma, R. Yu, D. Liu. Corros. Sci. 41 (1999) 1273-1287.

[22] Z. Quan, S. Chen, Y. Li, Corros. Sci. 43 (2001) 1071-1080.

[23] P. Singh, A.K. Singh, V.P. Singh, Polyhedron 65 (2013) 73–81.

[24] K.K. Narang, J.P. Pandey, V.P. Singh, Polyhedron 13 (1994) 529–538.

[25] G.H. Jeffery, J. Bassett, J. Mendham, R.C. Denney, Vogel's Textbook of Quantitative Chemical Analyses, fifth ed., Longman, Amsterdam, 1989.

[26] G.M. Sheldrick, Acta Crystallogr. Sect. A 46 (1990) 467–473.

[27] G.M. Sheldrick, SHELXL-97, Program for Crystal Structure Refinement, University of Gottingen, Germany, 1997.

[28] I.J. Bruno, J.C. Cole, P.R. Edgington, M. Kessler, C.F. Macrae, P. McCabe, J. Pearson, R. Taylor, Acta Crystallogr. Sect. B 58 (2002) 389–397.

[29] L.J. Farrugia, J. Appl. Crystallogr. 30 (1997) 565.

[30] A.D. Becke, J. Chem. Phys. 98 (1993) 5648–5652.

[31] G.A. Petersson, M.A. Al-Laham, J. Chem. Phys. 94 (1991) 6081-6090.

[32] P.J. Hay, W.R. Wadt, J. Chem. Phys. 82 (1985) 270-283.

[33] A.K. Singh, M.A. Quraishi, Int. J. Electrochem. Sci. 7 (2012) 3222-3241.

[34] V.L. Siji, M.R. Sudarsanakumar, S. Suma, Polyhedron 29 (2010) 2035–2040.

[35] J.C. Wu, S.X. Liu, T.D. Keene, A. Neels, V. Mereacre, A.K. Powell, S. Decurtins, Inorg. Chem. 47 (2008) 3452–3459.

[36] B. Mondal, T. Ghosh, M. Sutradhar, G. Mukherjee, M.G.B. Drew, T. Ghosh, Polyhedron 27 (2008) 2193–2201.

[37] S.A. Patil, S.N. Unki, A.D. Kulkarni, V.H. Naik, P.S. Badami, Spectrochim. Acta A 79 (2011) 1128-1136.

[38] F.A. Cotton, G. Wilkinson, C.A. Murillo, M. Bachmann, Advanced Inorganic Chemistry, sixth ed., Wiley, New York, (2003).

[39] A.B.P. Lever, Inorganic Electronic Spectroscopy, second ed., Elsevier, Amsterdam, 1984.

[40] A.K. Ghosh, K.K. Kamar, P. Paul, S.M. Peng, G.H. Lee, S. Goswami, Inorg. Chem. 41 (2002) 6343–6350.

[41] P. Krishnamoorthy, P. Sathyadevi, A.H. Cowley, R.R. Butorac, N. Dharmaraj, Eur. J. Med. Chem. 46 (2011) 3376–3387.

[42] P. Sathyadevi, P. Krishnamoorthy, R.R. Butorac, A.H. Cowley, N.S.P. Bhuvanesh, N. Dharmaraj, Dalton Trans. 40 (2011) 9690–9702.

[43] V. Mahalingam, N. Chitrapriya, M. Zeller, K. Natarajan, Polyhedron 28 (2009) 1532–1540.

[44] M.A. Ali, A.H. Mirza, R.J. Butcher, M.T.H. Tarafder, M.A. Ali, Inorg. Chim. Acta 320 (2001) 1-6.

[45] T. Birk, K.S. Pedersen, S. Piligkos, C.A. Thuesen, H. Weihe, J. Bendix, Inorg. Chem. 50 (2011) 5312–5314.

[46] F. Cisnetti, G. Pelosi, C. Policar, Inorg. Chim. Acta 360 (2007) 557-562.

[47] J.J. Vittal, X. Yang, Cryst. Growth Des. 2 (2002) 259–262.

[48] J.R. Dilworth, J. Hyde, P. Lyford, P. Vella, K. Venkatasubramaman, J.A. Zubieta, Inorg. Chem. 18 (1979) 268–274.

[49] A.K. Singh, M. Yadav, S.K. Singh, S. Sunkari, D.S. Pandey, Inorg. Chim. Acta 363 (2010) 995–1000.

[50] M. Maiti, D. Sadhukhan, S. Thakurta, S. Roy, G. Pilet, R. J. Butcher, A. Nonat, L. J. Charbonniere, S. Mitra, Inorg. Chem. 51 (2012) 12176−12187.

[51] K.R. Grunwald, M. Volpe, P. Cias, G. Gescheidt, N.C. Mosch-Zanetti, Inorg. Chem. 50 (2011) 7478–7488.

[52] I. Persson, P. Persson, M. Sandstrom, A.S. Ullstrom, J. Chem. Soc. Dalton Trans. (2002) 1256−1265.

[53] P.F. Barron, J.C. Dyason, P.C. Healy, L.M. Engelhardt, C. Packawatchai, V.A. Patrick, A.H. White, J. Chem. Soc. Dalton Trans. (1987) 1099−1106.

[54] D. Kalita, R.C. Deka, N.S. Islam, Inorg. Chem. Commun. 10 (2007) 45–48.

[55] I. Bytheway, M.W. Wong, Chem. Phys. Lett. 282 (1998) 219–226.

[56] M. Erbil, Chim. Acta Turc. 1 (1988) 59–70.

[57] V.P. Singh, P. Singh, A.K. Singh, Inorg. Chim. Acta 379 (2011) 56-63.

[58] M.A. Amin, S.S.A. El-Rehim, E.E.F. El-Sherbini, R.S. Bayoumi, Electrochim. Acta 52 (2007) 3588–3600.

Figure captions:

Fig. 1. ORTEP diagram of ligand showing atomic numbering scheme with ellipsoids of 30 % probability**.**

Fig. 2. ORTEP diagram of [Mn(Hhbpp)$_2$)] showing atomic numbering scheme with ellipsoids of 30% probability (the structure has crystallographic two-fold symmetry and symmetric atoms are generated by symmetry operation = -x+1, y, -z+3/2).

Fig. 3. ORTEP diagram of [Zn(hbpp)(DMSO)]$_2$ showing atomic numbering scheme with ellipsoids of 30% probability (the structure contains a crystallographic centre of symmetry and symmetric atoms are generated by symmetry operation = -x+2, -y, -z).

.**Fig. 4.** Optimized geometry of [Cu(Hhbpp)$_2$] using B3LYP method and 6-31g(d,p)/LANL2DZ basis sets (ORTEP view at 30% probability).

Fig. 5. (a) Nyquist plot, (b) Bode plot, (c) Phase angle plot in absence and presence of inhibitors and (d) Nyquist plot for mild steel in 1 M HCl solution in absence of inhibitor with proposed circuit fitted data; where Z_r is real impedance, Z_i is an imaginary part of impedance, θ is phase angle and f is frequency.

Fig. 6. The electrochemical equivalent circuit used to fit the impedance measurements that include a solution resistance (Rs), a constant phase element (CPE), a polarization resistance or charge transfer (Rct), inductance (L) and resistance due to inductive loop (R_L).

Fig. 7. Potentiodynamic polarizations for ligand and its metal(II) complexes.

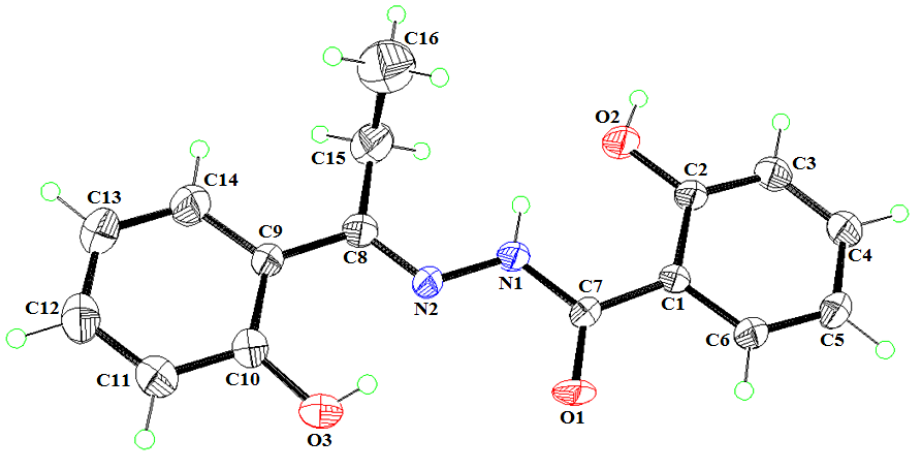

Fig. 1. ORTEP diagram of ligand showing atomic numbering scheme with ellipsoids of 30 % probability.

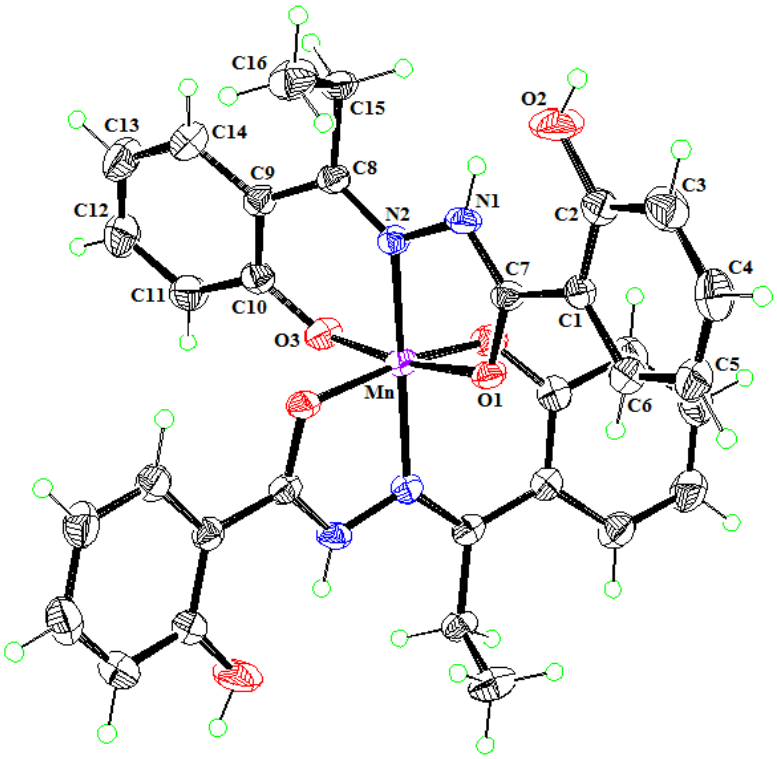

Fig. 2. ORTEP diagram of [Mn(Hhbpp)$_2$)] showing atomic numbering scheme with ellipsoids of 30% probability (the structure has crystallographic two-fold symmetry and symmetric atoms are generated by symmetry operation = -x+1, y, -z+3/2).

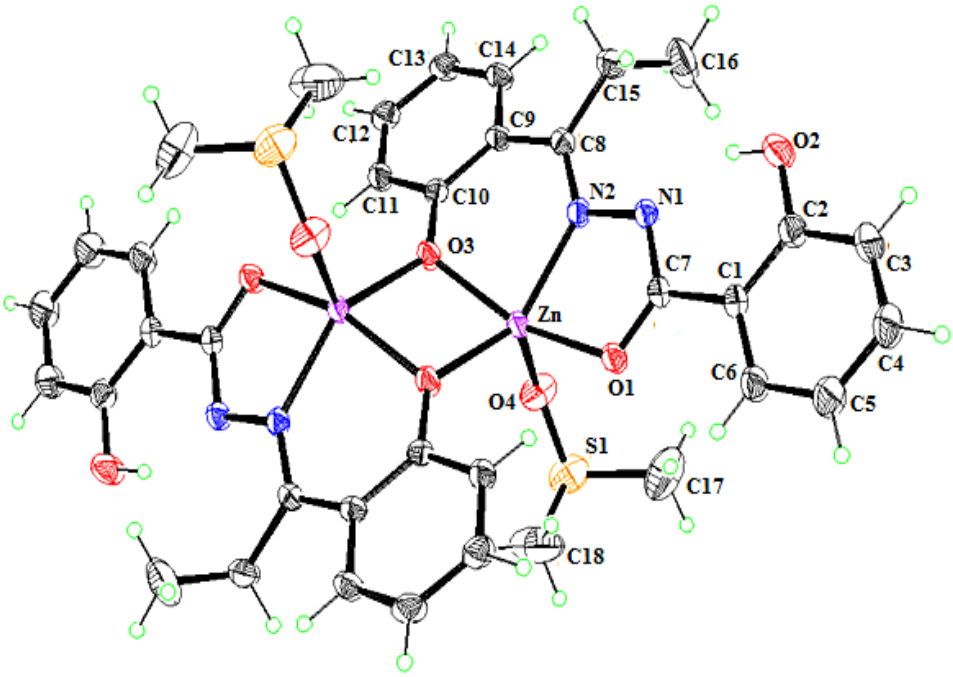

Fig. 3. ORTEP diagram of $[Zn(hbpp)(DMSO)]_2$ showing atomic numbering scheme with ellipsoids of 30% probability (the structure contains a crystallographic centre of symmetry and symmetric atoms are generated by symmetry operation = -x+2, -y, -z).

.

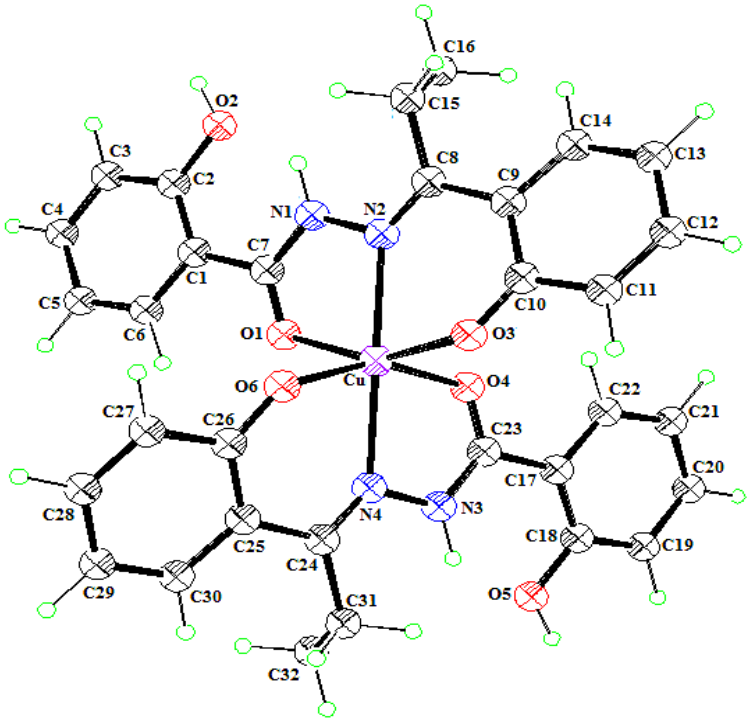

603

604

605 **Fig. 4.** Optimized geometry of [Cu(Hhbpp)$_2$] using B3LYP method and 6-
606 31g(d,p)/LANL2DZ basis sets (ORTEP view at 30% probability).

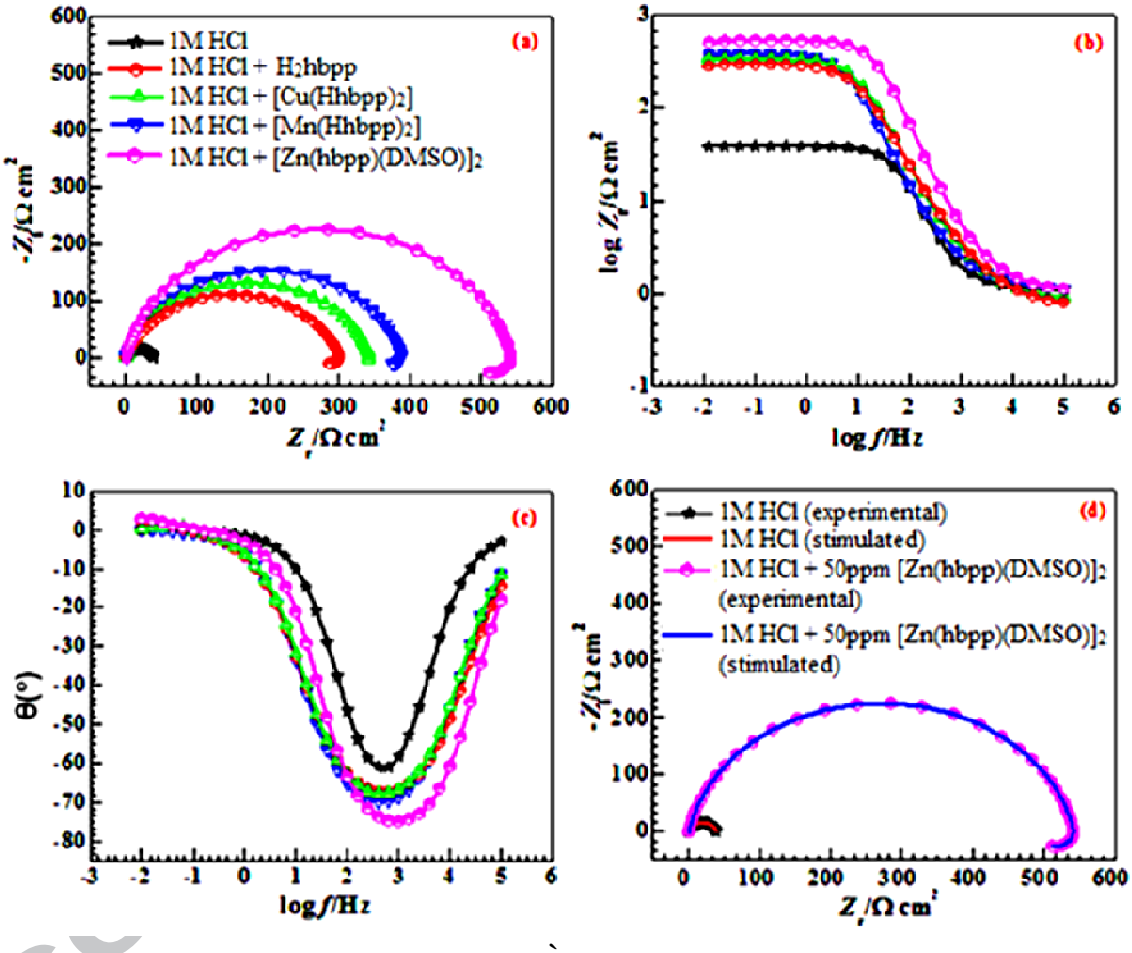

607
608

609 **Fig. 5.** (a) Nyquist plot, (b) Bode plot, (c) Phase angle plot in absence and presence of
610 inhibitors and (d) Nyquist plot for mild steel in 1 M HCl solution in absence of inhibitor with
611 proposed circuit fitted data; where Z_r is real impedance, Z_i is an imaginary part of impedance,
612 θ is phase angle and f is frequency.

613

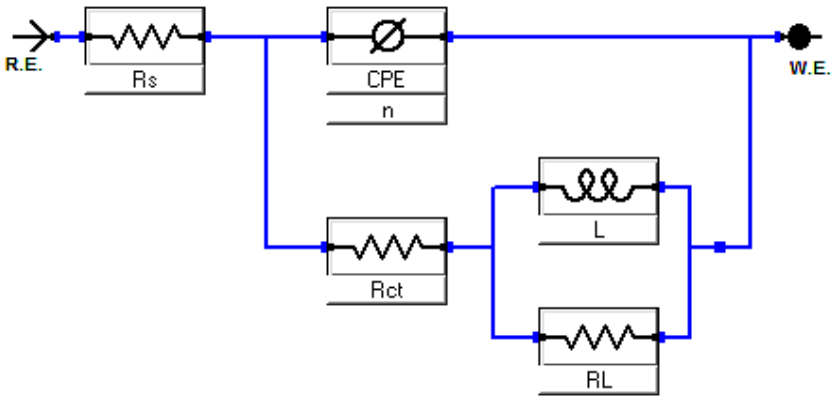

Fig. 6. The electrochemical equivalent circuit used to fit the impedance measurements that include a solution resistance (Rs), a constant phase element (CPE), a polarization resistance or charge transfer (Rct), inductance (L) and resistance due to inductive loop (R_L).

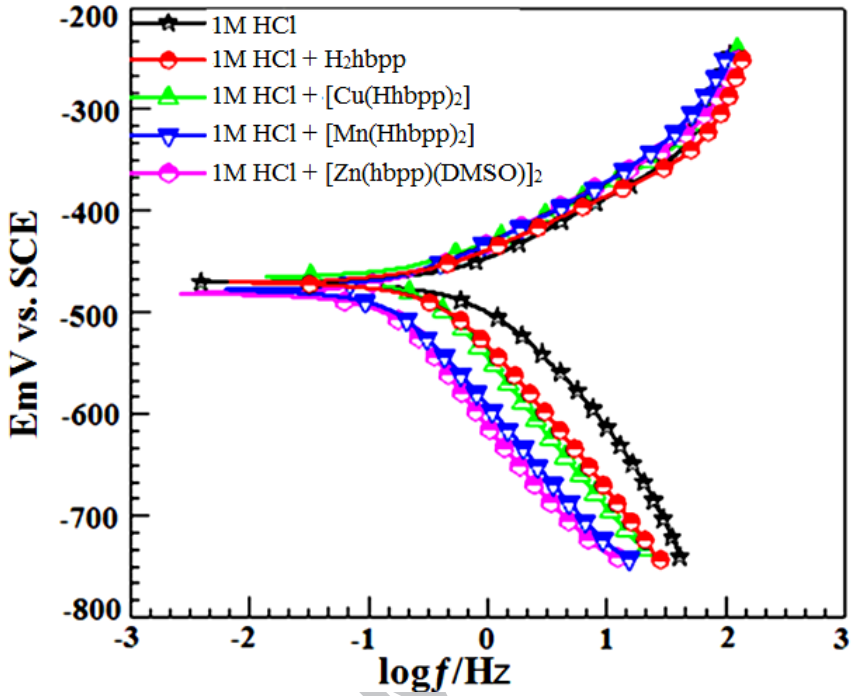

Fig. 7. Potentiodynamic polarizations for ligand and its metal(II) complexes.

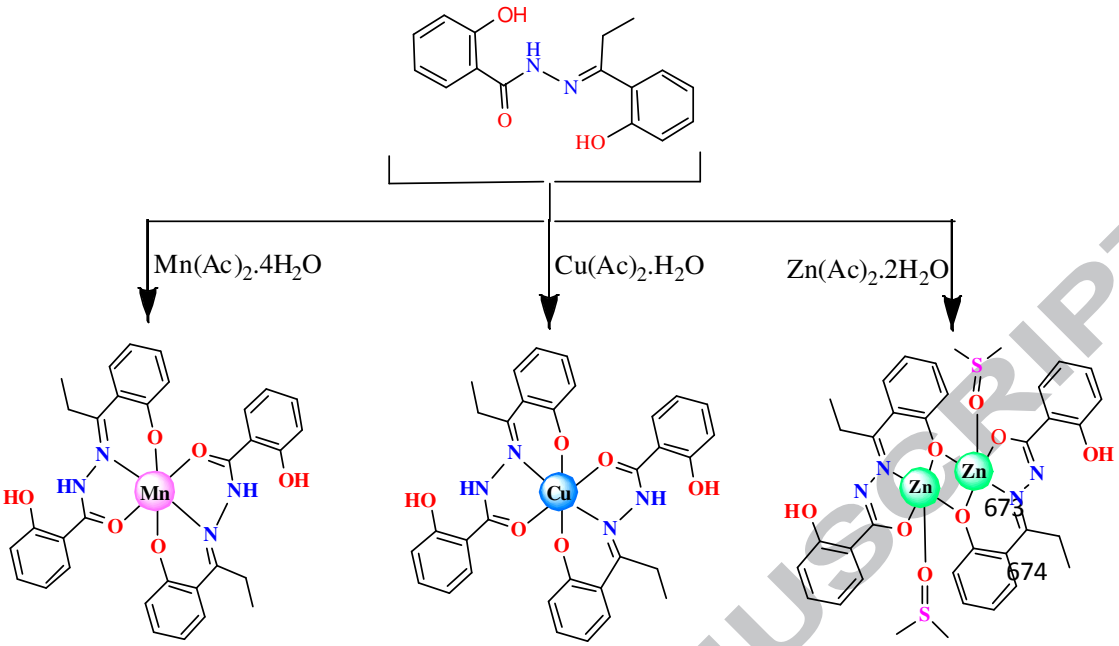

Scheme 1.

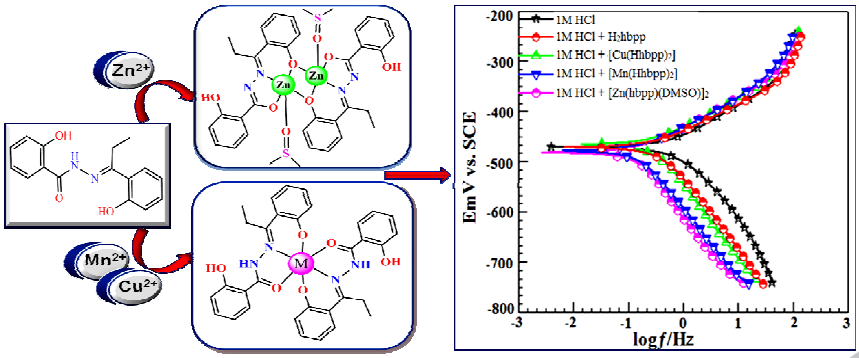

Mononuclear Mn(II), Cu(II) and phenoxo-bridged dimeric Zn(II) complexes of 2-hydroxy-benzoic acid[1-(2-hydroxy-phenyl)-propylidene]-hydrazide have been synthesized and characterized by different spectral and X-ray diffraction techniques. These compounds have also been analysed for corrosion-inhibition properties for mild steel in 1M HCl medium.